A R C H I V E S O F M E T A L L U R G Y A N D M A T E R I A L S
Volume 60 2015 Issue 2
DOI: 10.1515/amm-2015-0181

O. WYSOCKA-FOTEK*, M. MAJ*, W. OLIFERUK *,**,♯

USE OF PULSED IR THERMOGRAPHY FOR DETERMINATION OF SIZE AND DEPTH OF SUBSURFACE DEFECT TAKING INTO ACCOUNT THE SHAPE OF ITS CROSS-SECTION AREA

ZASTOSOWANIE IMPULSOWEJ TERMOGRAFII PODCZERWIENI DO SZACOWANIA WIELKOŚCI I POŁOŻENIA DEFEKTÓW PODPOWIERZCHNIOWYCH Z UWZGLĘDNIENIEM KSZTAŁTU ICH PRZEKROJÓW POPRZECZNYCH

The paper is devoted to reconstruction of size and depth (distance from the tested surface) of artificial defects with square and rectangular cross-section areas using the pulsed IR thermography. Defects in form of flat-bottom holes were made in austenitic steel plate. The defect size was estimated on the basis of surface distribution of the time derivative of the temperature. In order to asses the depth of defects with considered geometries on the basis of calibration relations (i.e. dependence of time of contrast maximum vs. defect depth for given defect diameter) obtained for circular defects, the 'equivalent diameter' describing not only the defect cross-section area but also its shape was assigned. It has been shown that presented approach gives satisfactory results.

Keywords: pulsed IR thermography, defect size, defect depth, cross-section shape of defect

Praca dotyczy wyznaczania wielkości i głębokości (odległości od badanej powierzchni) symulowanych defektów o przekroju kwadratowym i prostokątnym przy użyciu impulsowej termografii podczerwieni. Defekty, w formie nieprzelotowych otworów o płaskim dnie, wykonano w blasze ze stali austenitycznej. Wielkość defektów określano analizując powierzchniowy rozkład pochodnej temperatury względem czasu.

Aby wykorzystać zależności kalibracyjne (zależności czasu odpowiadającemu maksimum kontrastu temperatury od głębokości defektu o danej średnicy) dla defektów o przekroju kołowym do oszacowania głębokości defektów kwadratowych i prostokątnych, przyporządkowano im „ekwiwalentną średnicę" uwzględniającą nie tylko pole przekroju defektu, ale także kształt defektu. Pokazano, że dla rozpatrywanych geometrii defektów, zaproponowane podejście daje satysfakcjonujące rezultaty.

1. Introduction

Pulsed infrared (IR) thermography is one of active IR techniques in which a surface of tested material is stimulated by a short heat pulse and the thermal response of the material is analysed [1-11]. The response contains information about subsurface material defects. After the heat pulse the temperature decrease rate is different on surface over defect in comparison to that over the sound material. It is caused by a difference between values of thermal effusivity of the defected region and the sound one. The thermal effusivity of the given material is defined as:

$$e = \sqrt{k\rho c}, \tag{1}$$

where: k is thermal conductivity, ρ is a mass density and c is specific heat of the material. If the thermal effusivity of defect is lower than the effusivity of the matrix, the surface temperature over defect will be higher comparing to that over the sound material. As the quantitative measure of the difference between values of the surface temperature over defected zone and over the sound material the standard thermal contrast $C(t)$ is used [9]:

$$C(t) = \frac{T_{def}(t) - T_{def}(t_0)}{T_s(t) - T_s(t_0)}, \tag{2}$$

where T_{def} is the surface temperature over defect, T_S is the surface temperature over the sound material, t_0 is the time just before pulse heating and t is the current time of the cooling process.

It has been shown that the relation of thermal contrast vs. cooling time has a maximum [1, 7-15, 18-20]. But, the time related to the thermal contrast maximum is dependent on both size of defect and its depth [10-12]. In the literature, the time corresponding to thermal contrast maximum is often used for the defect depth determination [1, 7, 10-13, 15-20]. However, in most papers authors concern only defects of the same size located at the different depths [12-17, 19]. Such problem is easy to solve because it is not taking into account the conjugated effect of defect depth and size on the time of thermal contrast maximum. Nevertheless, our previous works have shown that the time of thermal contrast maximum can

* INSTITUTE OF FUNDAMENTAL TECHNOLOGICAL RESEARCH POLISH ACADEMY OF SCIENCES, WARSAW, POLAND
** BIALYSTOK UNIVERSITY OF TECHNOLOGY, BIALYSTOK, POLAND
♯ Corresponding author: wolif@ippt.gov.pl

be the same for different depths and sizes of defects [10, 11]. It means that in order to determine the defect depth on the basis of the time of thermal contrast maximum, it is necessary to know the defect size. In our previous works, the experimental methods of defect size and depth determination were proposed [10, 11]. The defect size was estimated on the basis of surface distribution of the time derivative of temperature, whereas the defect depth was assessed from the dependence of surface thermal contrast vs. cooling time. To reconstruct the defect depth using this method, the calibration relations are needed. These are relations between defect depth and the time of thermal contrast maximum for given defect diameters. Such calibration relations for subsurface defects in austenitic steel plate are presented in Fig. 1 [10, 11]. On the basis of these relations, the depth of defect of reconstructed diameter can be estimated.

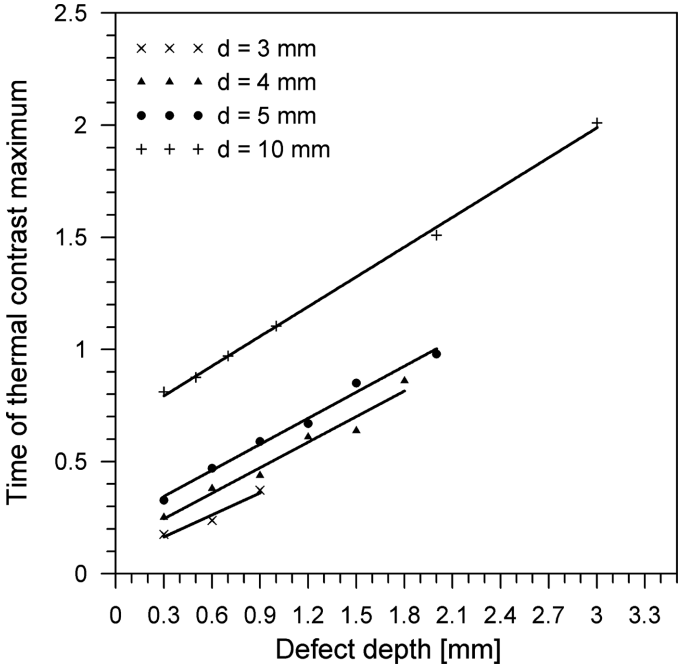

Fig. 1. Dependence of defect depth vs. time of thermal contrast maximum (the calibration relations)

However, the experiments have been performed, as in most other papers [1-4, 7, 8, 13, 15-20], on the specimen with artificial defects in form of the circular flat-bottom holes. Therefore, the question is: Whether the calibration relations obtained for circular defects could be used for depth determination of defects with different shape? In order to answer the question the experiments for square and rectangular defects were performed. Thus, the objective of this work is to reconstruct depth of square and rectangular defects on the basis of calibration relations obtained for circular defects.

2. Experimental procedure

The specimen made of 316L austenitic steel plate (190 mm x 290 mm x 6 mm) with square and rectangular artificial defects was prepared (Fig. 2).

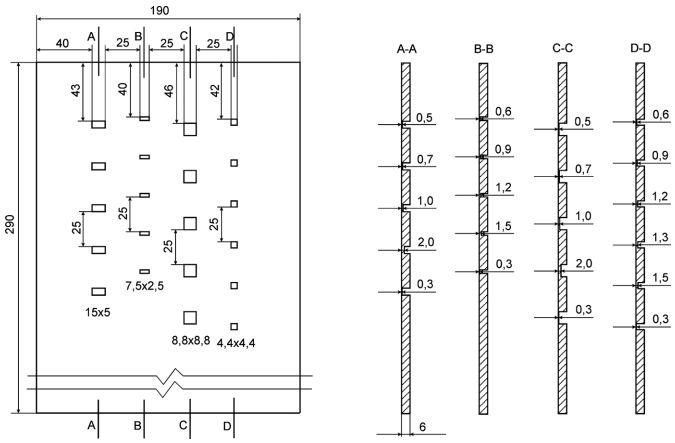

Fig. 2. The geometry of the steel plate with square and rectangular defects

The specimen was coated by graphite paint in order to ensure high and homogeneous surface emissivity. The surface of the specimen was uniformly heated using the halogen lamp of the pulse energy of 6 kJ. Pulse duration was 3 ms and the lamp to specimen distance was equal to 0.5 m. The surface temperature distribution vs. cooling time was measured by ThermaCam Phoenix infrared thermographic system with InSb detector. The spectral range of the detector was 3-5 mm. The thermal sensitivity of the system at 25°C is 20 mK. The thermal images (320×256 pixels) were recorded with the frequency 346 Hz. The IR camera and stimulating lamp were located at the same side of the specimen (Fig. 3).

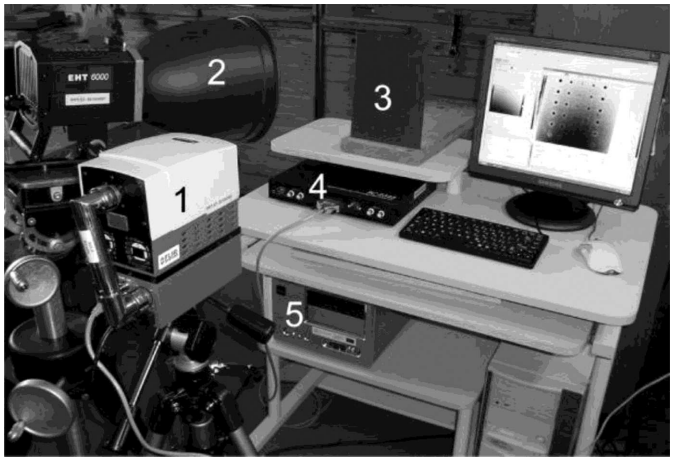

Fig. 3. Experimental set-up for pulsed thermography: 1 – IR camera, 2 – flash lamp, 3 – tested specimen, 4 – interface between IR camera and excitation lamp, 5 – computer

Both the material of the specimen and experimental conditions were the same as in case of the previous experiments performed for circular cross-sections of defects, for which the calibration relations were obtained [10].

3. Results

3.1. The standard thermal contrast determination

Using the procedure described in our previous work, the thermal contrasts (Eq. 2) vs. cooling time for artificial defects

of different size and depth were calculated on the basis of time dependence of temperature distribution [10]. It should be noticed that the obtained results are reliable only when the temperature distribution on the tested surface is not influenced by the opposite surface of the specimen. The range of cooling time, when there is no such influence, was obtained [10]. It has been shown that non-defected austenitic plate (thickness of 6 mm) can be treated as semi-infinite body up to the cooling time of 3 s. In other words, in this period the thermal contrast on the tested surface is not influenced by the opposite surface. In the present work, only these artificial defects were taken into account for which the time of the thermal contrast maximum was not greater then 3 s.

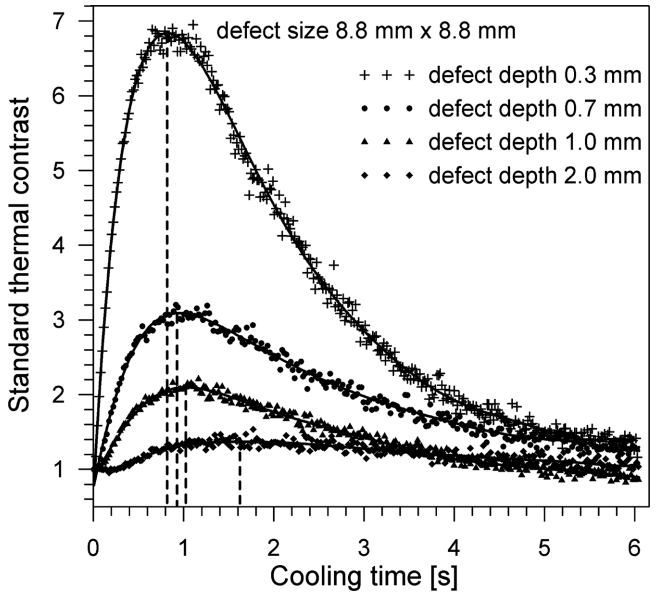

Fig. 4. Time evolution of the standard thermal contrast. Defect size is equal to 8.8 mm×8.8 mm

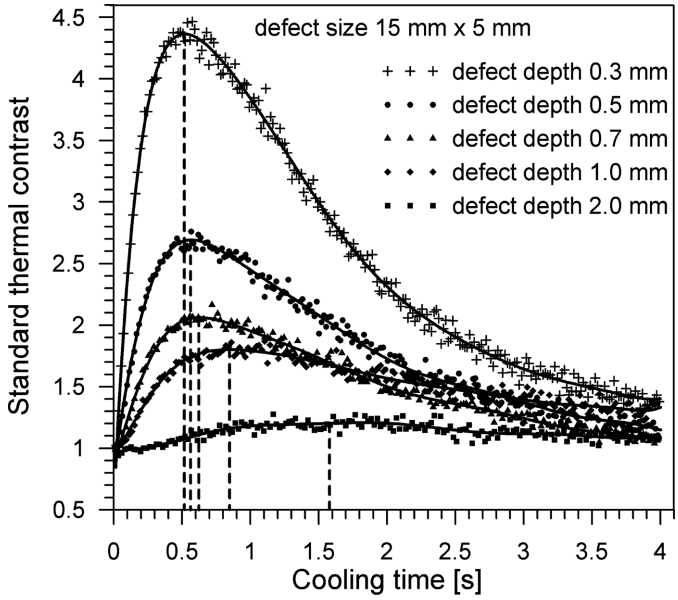

Fig. 5. Time evolution of the standard thermal contrast. Defect size is equal to 15 mm×5 mm

In Figs.: 4 and 5 the thermal contrast vs. cooling time for the defects size of 8.8 mm×8.8 mm and 15 mm×5 mm located at the different depths are presented. It is seen that the smaller depth of the defect corresponds to higher value of thermal contrast maximum and the shorter time to reach the maximum.

3.2. The defect size and depth determination

It was mentioned, that in order to determine the defect depth on the basis of calibration relations it is necessary to know the defect size. Using the procedure presented in our previous work, the size of square and rectangular defects was determined from the surface distribution of the time derivative of the temperature [10, 11]. An example of such distribution is presented in form of a gray field in Fig. 6. The grey levels (from 0 to 255 conventional dimensionless units) were assigned to the particular values of time derivative of temperature. Level 0 corresponds to black and the 255 to white colour. The distribution of gray level along horizontal and vertical axis pass through the centre of the visible trace of selected defect is presented in Figs: 7-8.

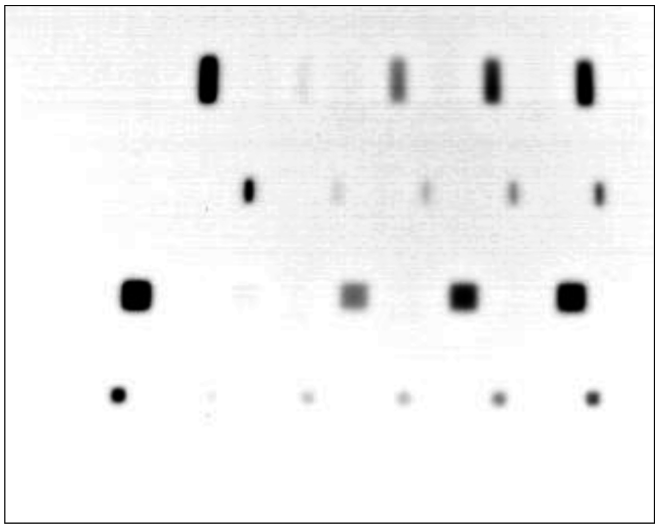

Fig. 6. Surface distribution of the time derivative of temperature, at the 0.67 s after heat pulse

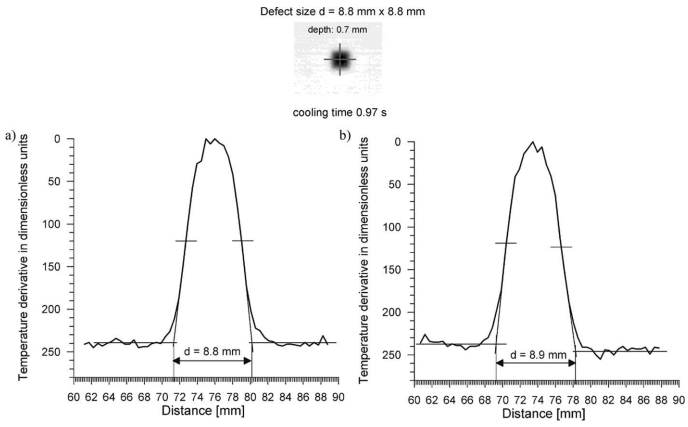

Fig. 7. Line profile of the time derivative of the temperature along a) horizontal axis and b) vertical axis, pass through the centre of the visible trace of defect size 8.8 mm×8.8 mm located at the depth 0.7 mm

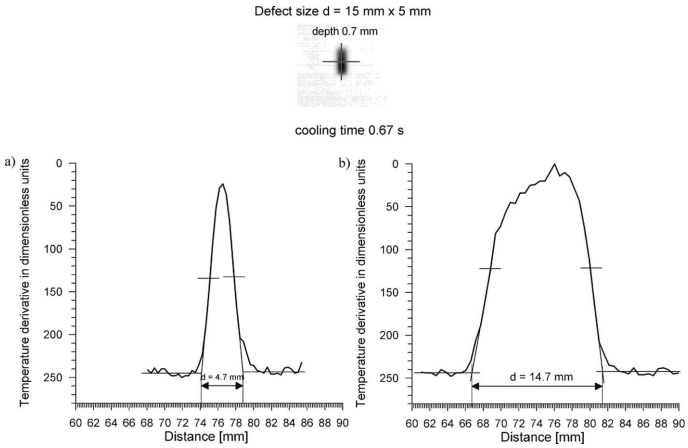

Fig. 8. Line profile of the time derivative of the temperature along a) horizontal axis and b) vertical axis, pass through the centre of the visible trace of defect size 15 mm×5 mm located at the depth 0.7 mm

TABLE 1
Comparison of reconstructed defect sizes with real ones

Defect depth [mm]	Reconstructed defect size [mm×mm]	Real defect size [mm×mm]
0.3	4.4×4.4	4.4×4.4
0.6	4.4×4.5	
0.9	4.5×4.4	
1.2	4.5×4.3	
1.3	4.3×4.3	
1.5	4.3×4.3	
0.3	8.8×8.8	8.8×8.8
0.5	8.9×8.9	
0.7	8.9×8.8	
1.0	8.9×8.9	
2.0	9.0×9.0	
0.3	7.5×2.5	7.5×2.5
0.6	7.5×2.6	
0.9	7.6×2.6	
1.2	7.45×2.6	
1.5	–	
0.3	15.0×5.1	15.0×5.0
0.5	15.0×5.1	
0.7	14.7×4.7	
1.0	14.9×5.2	
2.0	14.8×4.9	

Taking into account the IR camera to specimen distance and lens parameters, the horizontal and vertical pixel size were calculated. In order to determine the defect size the tangents to the both profile arms at the half of its height were drawn (see Figs.: 7 and 8). The distance between intersection points of these tangents with the lines related to the average values of temperature derivative over the sound material was taken as the defect size. Linear profiles of the time derivative of temperature were determined for the time corresponding to thermal contrast maximum. This time is different for different sizes and depths of defects. The comparison of the reconstructed values of defect size with real ones is presented in Table 1.

It should be noticed that, the reconstruction of the defect size is impossible if the increase in thermal contrast is unnoticeable.

It has been shown that in case of circular defect of known diameter, the defect depth can be easily estimated from adequate calibration relation, i.e. dependence of time of thermal contrast maximum on defect depth for given diameter [10, 11]. In order to use such calibration relations for non-circular defects, it is necessary to assign them some diameter. However, the comparison of results obtained for circular, square and rectangular defects with almost equal cross-section areas has shown that use of equivalent diameter (calculated from defect cross-section area) gives not satisfactory results (Fig. 9). It is seen that time of thermal contrast maximum depends not only on defect cross section area but also on its shape. It means that calibration relations obtained for circular defects can not be used for equivalent diameter of non-circular ones. Therefore, it is necessary to take into account the defect shape. In order to do that the following procedure was proposed. At first, the circle was inscribed and circumscribed in a given defect.

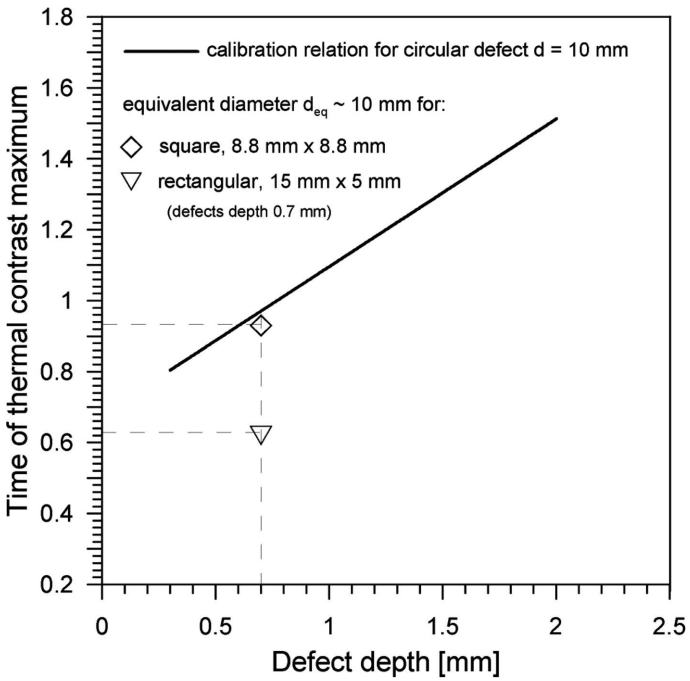

Fig. 9. Different times of thermal contrast maximum for exemplary non-circular defects with equal equivalent diameters. The calibration relation for circular defects is marked

Then, the average area of both circles were calculated and multiplied by the ratio of inscribed and circumscribed circle radius: $\left[\left(\frac{\pi r^2+\pi R^2}{2}\right)\cdot\frac{r}{R}\right]$. This term, describing area of a new circle, allows taking into account not only the defect cross-section area but also the defect shape. Then, for such area, the corresponding diameter ϕ was assigned:

$$\phi = 2\sqrt{\frac{\left[\left(\frac{\pi r^2+\pi R^2}{2}\right)\cdot\frac{r}{R}\right]}{\pi}} = \sqrt{2\left(r^2+R^2\right)\cdot\frac{r}{R}}. \qquad (3)$$

The diameter ϕ for rectangular defect is schematically shown in Fig. 10.

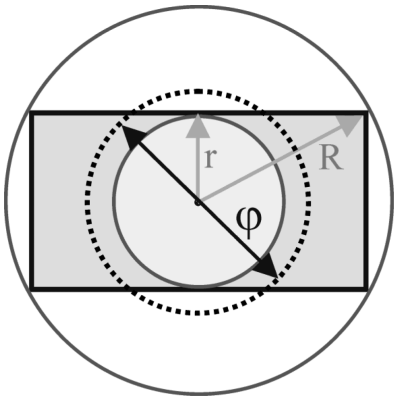

Fig. 10. Circles inscribed and circumscribed in the rectangular defect. The diameter ϕ, taking into account both the defect cross-section area and its shape, is marked

Using presented method the diameters ϕ for all square and rectangular defects were determined. Then, using obtained values of ϕ the depths of the square and rectangular defects were determined from calibration relations for defects of circular cross-sections. An example of depth estimation for rectangular defect (15 mm×5 mm) is presented in Fig 11.

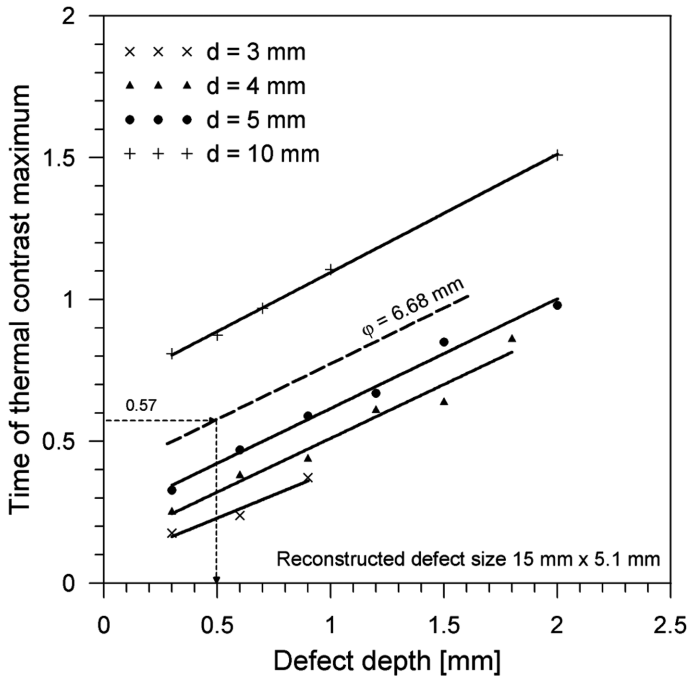

Fig. 11. An example of determination the depth of rectangular defect (15 mm×5 mm) on the basis of calibration relations obtained for defects of circular cross-section

For this defect, the obtained value of ϕ is equal to 6.68 mm and the time corresponding to maximum of thermal contrast is equal to 0.57 s. The depth estimated on the basis of calibration relations is equal to 0.5 mm. As it is seen, the obtained value is equal to real defect depth (Fig. 11). Results for all defects compared with real defect depths are presented in Table 2. It is seen that presented approach gives satisfactory results.

TABLE 2
Comparison of reconstructed defect depths with real ones

Reconstructed defect size [mm×mm]	φ [mm]	Reconstructed defect depth [mm×mm]	Defect depth [mm]
4.4×4.4	4.53	0.30	0.3
4.4×4.5	4.54	0.60	0.6
4.5×4.4	4.54	0.90	0.9
4.5×4.3	4.45	1.35	1.2
4.3×4.3	4.43	1.50	1.3
4.3×4.3	4.43	1.75	1.5
8.8×8.8	9.06	0.37	0.3
8.9×8.9	9.17	0.50	0.5
8.9×8.8	9.07	0.90	0.7
8.9×8.9	9.17	1.30	1.0
9.0×9.0	9.27	2.30	2.0
7.5×2.5	3.30	0.25	0.3
7.5×2.6	3.38	0.47	0.6
7.6×2.6	3.40	0.80	0.9
7.45×2.6	3.37	1.39	1.2
–	–	–	1.5
15.0×5.1	6.68	0.32	0.3
15.0×5.1	6.68	0.50	0.5
14.7×4.7	6.29	0.74	0.7
14.9×5.2	6.74	1.28	1.0
14.8×4.9	6.47	2.53	2.0

4. Conclusion

Determination of the defect depth from calibration relations (dependences between defect depth and time of thermal contrast maximum for given defect diameters) require to know the defect size and the time of thermal contrast maximum. The size of square and rectangular defects was assessed from the surface distribution of the time derivative of the temperature.

To use the calibration relations obtained for defects of circular cross-section to estimate the depth of defects of different cross-section should be introduce the quantity taking into account the cross-section shape of defect. This quantity is defined as:

$$\sqrt{2\,(r^2 + R^2) \cdot \frac{r}{R}}.$$

The values of ϕ has been used to reconstruct the depth of square and rectangular defect with different sizes and depths made in austenitic steel plate. It has been shown that presented approach gives satisfactory results.

The presented experimental results may be helpful to validate numerical heat transfer model for specimen with subsurface defects. Such numerical models allow to analysis of defects of different geometries and orientations with respect to the tested surface without performing expensive and laborious

experiments. The obtained experimental results may also be used to solve the inverse problem by the numerical approach.

REFERENCES

[1] H.D. Benitez, C. Ibarra-Castanedo, A.H. Bendada, X. Maldague, H. Loaiza, E. Caicedo, Infrared Phys. Techn. **51**, 160-167 (2008).

[2] D.A. Gonzalez, C. Ibarra-Castanedo, J.M. Lopez-Higuera, X. Maldague, Nondestruct. Test. Eva. **39**, 617-621 (2006).

[3] M. Pilla, M. Klein, X. Maldague, A. Salerno, in: D. Balageas, G. Busse, G.M. Carlomagno, S. Svaić (Ed.), 6th International Conference Quantitative Infrared Thermography, Croatia, 53-58 (2002).

[4] S.M. Shepard, J.R. Lhota, Y. Hou, T. Ahmed, Insight **46**, 210-213 (2004).

[5] S. Lungin, U. Netzelmann, Nondestruct. Test. Eva. **38**, 485-490 (2005).

[6] S. Lungin, U. Netzelmann, Nondestruct. Test. Eva. **40**, 220-228 (2007).

[7] J.G. Sun, J. Heat Transf. **128**, 329-338 (2006).

[8] A.R. Hamzah, P. Delpech, M.B. Saintey, D.P. Almond, Insight **38**, 167-171 (1996).

[9] X.P.V. Maldague, Willey-Interscience, Theory and practice of infrared technology for nondestructive testing, New York 2001.

[10] O. Wysocka-Fotek, W. Oliferuk, M. Maj, Infrared Phys. Techn. **55**, 363-367 (2012).

[11] M. Maj, W. Oliferuk, O. Wysocka, in. B. Więcek (Ed.), 9th International Conference on Quantitative Infrared Thermography, Poland, 627-631 (2008).

[12] M. Suśa, Numerical modelling of pulse thermography experiments using finite elements for purposes of defect characterization. PhD thesis, University Laval, Quebec.

[13] C. Deemer, J.G. Sun, W.A. Ellington, S. Short, OSTI ANL/ET/CP-97040, 1-7 (1999).

[14] H.X. Favro, X. Han, Y. Wang, P.K. Kou, R.L. Thomas, in: D.O. Thompson, D.E. Chimenti (Ed.), Review of Progress in Quantitative Nondestructive Evaluation, Plenum Press, New York, 425-430 (1995).

[15] V.P. Vavilov, T. Ahmed, H.J. Jin, L.R. Favro, L.D. Thomas, Experimental thermal tomography of solids by using the pulse one-side heating, Sov. J. Nondestruct. Test. **12**, 60-66 (1990).

[16] I. Boras, S. Svaic, A. Galovic, in: D. Balageas, G. Busse, G.M. Carlomagno (Ed.), 4th International Conference on Quantitative Infrared Thermography, Studio Poligraficzne M.Color, Poland (1998).

[17] I. Boras, S. Slavic, International Symposium Non-Destructive Testing in Civil Engineering, in.: (Ed.), Berlin (2003).

[18] S.K. Lau, D.P. Almond, J.M. Milne, Nondestruct. Test. Eva. **24**, 195-202 (1991).

[19] Y.A. Plotnikov, W.P. Winfree, in: D.O Thompson, D.E. Chimenti (Ed.), Review of Progress in Quantitative Nondestructive **19**, Canada (1999).

[20] H.I. Ringermacher, J.R. Archacki, W.A. Veronesi, U.S. Patent No. 5, 711, 603 (1998).

Received: 20 September 2014.